Method for continuous clustering of helicopter turboshaft engine's short-term gas temperature fluctuations to assess the compressor turbine element's degradation

Serhii Vladov[1,*,†], Victoria Vysotska[1,†], Maria Pysmenna[2,†], Andrii Nevynitsyn[2,†], Nataliia Vladova[1,2,†], Volodymyr Mazharov[2,†], Nadiia Kovalenko[2,†], Artem Zelenskyi[2,†] and Łukasz Ścisło[3,†]

[1] *Kharkiv National University of Internal Affairs, L. Landau Avenue 27, 61080 Kharkiv, Ukraine*
[2] *Ukrainian State Flight Academy, Chobanu Stepana Street 1, 25005 Kropyvnytskyi, Ukraine*
[3] *Cracow University of Technology, Warszawska 24, 31-155 Craków, Poland*

Abstract

This paper develops and verifies a streaming method for continuously clustering the helicopter turboshaft engine's gas temperature in front of the compressor turbine short-term fluctuations to assess the initial stages of the first-stage turbine blade degradation connected to the compressor. The developed method includes a signal quality control and imputation module, adaptive baseline detrending, local robust normalization, multifunctional feature extraction in sliding windows, online dimensionality reduction, and incremental clustering with exponential "forgetting" and dynamic component lifecycle management. An expert-calibrated "cluster → physical degradation signature" map and an aggregated scalar metric based on the assignments' sliding fraction to a defective cluster are introduced for prompt alerting. The method assesses the first-stage turbine blades' degradations' initial stages connected to the compressor. The developed method was validated using TV3-117 engine flight data (1280 samples at 4 Hz) and simulated scenarios (drift, transient spikes, increased noise, flatline, and regime change). Based on the experimental results, a reproducible "defective" cluster signature was identified (increased window average and increased short-term variability). The defective assignments' sliding fraction consistently exceeded the 0.20 empirical threshold in the degradation models, ensuring early and interpretable warnings with a controlled false alarm rate.

Keywords

Continuous clustering, short-term temperature fluctuations, gas temperature in front of the compressor turbine, TV3-117 turboshaft engine, first-stage turbine blade defect, streaming data processing, time series analysis, online diagnostics, predictive maintenance, anomaly detection.

1. Introduction

It is known that helicopter turboshaft engines (TE) place high demands on the reliability and accuracy of operating parameter monitoring, since the compressor and compressor turbine component degradation directly affect thrust, fuel efficiency, and flight safety [1–3]. One of the most informative indicators of engine condition is the gas temperature in front of the compressor turbine, since its dynamics reflect changes in combustion modes, the blade's aerodynamic efficiency loss, and the possible formation of localized overheating [4–6]. Modern onboard sensors record the temperature value every 2 seconds (sampling frequency of 0.5 Hz), which provides sufficient resolution to capture short-term fluctuations accompanying the degradations' initial

AIT&AIS'2025: International Scientific Workshop on Applied Information Technologies and Artificial Intelligence Systems, December 18–19 2025, Chernivtsi, Ukraine
[1,*] Corresponding author.
[†] These authors contributed equally.
serhii.vladov@univd.edu.ua (S. Vladov); victoria.a.vysotska@lpnu.ua (V. Vysotska); mari.pismennaya.83@ukr.net (M. Pysmenna); nevatse@ukr.net (A. Nevynitsyn); nataliia.vladova@sfa.org.ua (N. Vladova); mazharov_volodymyr@sfa.org.ua (V. Mazharov); nadinkovalenko508@gmail.com (N. Kovalenko); zelenskyi.artem7@gmail.com (A. Zelenskyi); lscislo@pk.edu.pl (Ł. Ścisło)
0000-0001-8009-5254 (S. Vladov); 0000-0001-6417-3689 (V. Vysotska); 0000-0003-4509-8147 (M. Pysmenna); 0000-0001-7000-4929 (A. Nevynitsyn); 0009-0009-7957-7497 (N. Vladova); 0000-0002-9535-0841 (V. Mazharov); 0000-0002-1651-9750 (N. Kovalenko); 0009-0009-7044-8939 (A. Zelenskyi); 0000-0002-7365-8888 (Ł. Ścisło)

stages but simultaneously creates a non-stationary and noisy time series large enough to require special analysis methods [7, 8].

Traditional diagnostic approaches, such as [9, 10], often rely on thresholds, averaged values, or periodic inspections, which hinders the early detection of slowly progressing defects and low-amplitude anomalies manifested as short-term spikes or variable patterns. A flight mode instability, the external conditions' influence, and the annotated data's lack of real failures make the task particularly challenging. Methods with rigid model binding are either too sensitive to noise or lose information content with frequent mode changes [11, 12]. In such conditions, a continuous, online-oriented algorithm capable of identifying repetitive and rare patterns in streaming two-second data appears to be a promising tool for increasing diagnostic sensitivity.

Based on the above, a method for continuous clustering of helicopter TE's short-term gas temperature fluctuations in front of the compressor turbine development is aimed at generating robust, adaptive feature representations and cluster evolution metrics that link pattern distribution changes to the compressor and turbine components' physical degradation. The proposed approach ensures early detection of deviations without the need for extensive tagging, increases resilience to noise and temporal non-stationarity, and enables a transition from reactive to predictive maintenance. Furthermore, it is noted that the research practical significance lies in the potential reduction in operating costs and improved flight safety through the timely identification of the compressor turbine blade degradation's' initial stages, thereby optimizing maintenance intervals.

2. Related Works

The importance of monitoring the gas temperature in front of the compressor turbine for helicopter TE diagnostics has long been recognized, since its dynamics closely correlate with changes in the gas-air tract (compressor performance, combustion efficiency, local overheating) and it is often used as a key engine parameter [13]. This is the basis for both classical approaches to detecting degradation (EGT margin, basic predictive models) [14–17] and modern data-driven solutions [18–20].

Currently, there are three main areas of diagnostic approaches, which include thermodynamic methods, such as [21, 22], and threshold algorithms, such as [23, 24], and statistical and machine learning models used to construct a gas temperature values "baseline" and detect deviations. Among them, popular ones are regression methods [25, 26], autoencoders [27, 28], decision trees [29, 30], and boosting methods [31, 32], as well as complex digital twins [33] and deep neural network architectures, including LSTM [34, 35], Transformer models [36, 37], and hybrid solutions, such as [38–40], used to predict degradation and estimate the remaining service life. Recent studies demonstrate the significant potential of digital twins and deep neural networks for accurately modeling degradation processes. At the same time, these methods place increased demands on the correct normalization of data and accounting for changes in operating modes.

One of the main challenges is the temporal variability of operating conditions (flight mode changes, load changes, external conditions) and the low-amplitude presence, short-term bursts in gas temperature, which traditional averaging methods and threshold detectors either ignore or mistake for noise. Recent studies, such as [41–43], highlight the need for methods that are robust to time-varying conditions. For example, spectral equalization normalization and self-tuning preprocessing improve the neural networks training under changing conditions, but do not fully solve the problem of identifying short, repeating patterns in data streams.

It is noted that in recent years, studies have appeared that use cluster analysis [44] and matrix profile-based methods [45] to detect anomalies and recurring patterns in time series (including cluster-aware modifications). These approaches are good for detecting typical patterns and local anomalies without explicit labeling; however, most implementations are designed for batch processing or focused on relatively long signal fragments (vibrations, power), rather than streaming (online) processing of gas temperatures' high-frequency short bursts with a 0.5 Hz

frequency. Furthermore, cluster-oriented matrix profile solutions rarely directly link cluster evolution to the physical degradation of the helicopter TE compressor turbine blade.

Some recent studies, such as [46], propose adaptive neural network and hybrid methods for local problems (signal reconstruction, adaptive predictive filtering), but empirical studies focusing specifically on continuous clustering of two-second gas temperature flows and their interpretation in helicopter TE compressor turbine blade degradation terms bremain insufficient. Furthermore, measurement reliability issues (dual thermocouples, data gaps, signal reconstruction) under helicopter flight conditions complicate the application of purely algorithmic solutions.

Thus, based on the above, a number of key unresolved issues have emerged, justifying the need to develop a method for continuous clustering of gas temperature short-term fluctuations in helicopter TE. Key among these is the need for reliable detection and stable extraction of low-amplitude, short-term patterns amid significant fluctuations in operating conditions. Furthermore, existing studies lack mechanisms for online adaptation to operating mode changes without requiring full retrainability of models. Furthermore, it is necessary to consider the onboard platform's computational limitations, including limited resources and latency requirements, which dictate the requirements for the solution's computational efficiency. Finally, with a limited number of labeled failure examples, semi- and unsupervised validation approaches are needed to assess the cluster shift's significance for substantiating technical maintenance decisions.

Therefore, each of these issues cannot be addressed using existing batch, supervised, or "basic" clustering approaches without specially developed online clustering mechanisms, adaptive normalization, a cluster evolution tracking mechanism, and procedures for linking cluster changes to physical degradation models. Therefore, developing a continuous clustering method focused on helicopter TE two-second temperature flows for assessing compressor turbine blade degradation is a pressing scientific and practical challenge.

3. Materials and Methods

The proposed method for continuous clustering of helicopter TE short-term temperature fluctuations in front of the compressor turbine is formalized as a dataflow algorithm that accepts as input a scalar time series of measurements $x_n = x(t_n)$, where $t_n = t_0 + 2 \cdot n$ with a sampling step of $\Delta t = 2$ seconds. A window of m samples (window time $T_w = 2 \cdot m$ seconds) and a sliding step s (in samples) are introduced. Data flow processing is defined by the operation $S_n = \{xn - m + 1, \ldots, x_n\}$. Primary preprocessing is reduced to baseline reconstruction and slow-time component suppression, within which the baseline is estimated by an exponential moving average

$$b_n = \alpha \cdot x_n + (1-\alpha) \cdot b_{n-1} \tag{1}$$

and subtract it, obtaining the detrended signal $\tilde{x}_n = x_n - b_n$. To ensure robustness to outliers, robust normalization based on the median and MAD is used [47, 48]:

$$med_n = median(S_n), \quad MAD_n = median(|x - med_n|), \quad z_n = \frac{x_n - med_n}{MAD_n + \epsilon}. \tag{2}$$

When data is missing, local imputation is applied, which is a linear interpolation or a model regressor. When detecting "sticking" or artifacts, a zero-variance check is introduced for the window. That is, if $\mathrm{Var}(S_n) < \delta$, the signal is flagged as suspected sensor failure and reconstructed by approximating the previous adequate windows. Each window S_n is mapped into a feature space $\mathbb{R}^d$ with a feature set combining statistics, differential, and spectral characteristics. A typical feature vector is represented as:

$$\phi(S_n) = \left[\mu_n, \sigma_n^2, \gamma_n, \kappa_n, max(S_n), min(S_n), \frac{d\bar{x}_n}{dt}, \frac{d^2\bar{x}_n}{dt^2}, c_{vsf} \right], \tag{3}$$

where $\mu_n = \frac{1}{m} \cdot \sum_{i=1}^{m} x_{n-m+i}$, σ_n^2 is the dispersion, γ_n, κ_n are the asymmetry and excess coefficients, $\frac{d\bar{x}_n}{dt}$ and $\frac{d^2\bar{x}_n}{dt^2}$ are the gas temperature first and second derivatives over time average values, cvsf is the continuous wavelet transform scale coefficients vector.

The cluster core is implemented as an incremental mixture of K components with parameters . For assignment and updating, a stochastic gradient is used to maximize the Gaussian mixtures' partial likelihood [49]. At the feature input step ϕ_t, prior weights and responsibilities are calculated as:

$$r_{j,t} = \frac{\pi_{j,t-1} \cdot N\left(\phi_t \middle| \mu_{j,t-1}, \Sigma_{j,t-1}\right)}{\sum_{k=1}^{K} \pi_{k,t-1} \cdot N\left(\phi_t \middle| \mu_{k,t-1}, \Sigma_{k,t-1}\right)}. \quad (4)$$

The parameter update is performed with exponential forgetting $\lambda \in (0, 1)$ as:

$$N_{j,t} = \lambda \cdot N_{j,t-1} + r_{j,t}, \mu_{j,t} = \frac{\lambda \cdot N_{j,t-1} \cdot \mu_{j,t-1} + r_{j,t} \cdot \phi_t}{N_{j,t}},$$

$$\Sigma_{j,t} = \frac{\lambda \cdot N_{j,t-1} \cdot \Sigma_{j,t-1} + r_{j,t} \cdot \left(\phi_t - \mu_{j,t}\right) \cdot \left(\phi_t - \mu_{j,t}\right)^T}{N_{j,t}} + \varepsilon \cdot I. \quad (5)$$

A priori weights are normalized as:

$$\pi_{j,t} = \frac{N_{j,t}}{\sum_k N_{k,t}}. \quad (6)$$

The proposed mechanism ensures adaptation to the feature distribution's evolution and the old pattern's forgetting. For non-degenerate distributions and automatic addition (or removal), the component is supplemented with procedures for creating new clusters under low density conditions:

$$\max_j N\left(\phi_t \middle| \mu_{j,t-1}, \Sigma_{j,t}\right) < \tau_{new}. \quad (7)$$

A new component is created with initial parameters

$$\mu_{new} = \phi_t, \Sigma_{new} = \sigma_n^2 \cdot I, N_{new} = N_0, \quad (8)$$

weak components are removed when $N_{j,t} < \tau_{del}$. To reduce the sensitivity to the distribution's shape, it is permissible to use the density distance based on the Mahalanobis distance [50]:

$$d_j\left(\phi_t\right) < \sqrt{\left(\phi_t - \mu_{j,t}\right)^T \cdot \Sigma_{j,t}^{-1} \cdot \left(\phi_t - \mu_{j,t}\right)}. \quad (9)$$

The anomalousness and associated degradation score are formulated as a hybrid score that takes into account the distance from the nearest cluster, local density, and the change in cluster occupancy rates over time. The anomalous score is defined as:

$$A\left(\phi_t\right) = \min_j \left(d_j\left(\phi_t\right)\right) \cdot \exp\left(-\beta \cdot \log\left(\pi_{j,t} + \varepsilon\right)\right), \quad (10)$$

where $\beta > 0$ scales the density contribution. To aggregate trends, a cluster share aggregation window is introduced

$$P_j(\tau) = \frac{1}{T} \cdot \int_{t-\tau}^{t} l\left\{assign\left(\phi_s\right) = j\right\} ds, \quad (11)$$

or, in discrete form,

$$P_{j,t} = \frac{1}{W} \cdot \sum_{i=t-W+1}^{t} l\left\{\arg\max_k \left(r_{k,i}\right) = j\right\}. \quad (12)$$

In the cluster evolution metric D (drift), the divergence between distributions in two adjacent intervals is used:

$$D(t_1,t_2)=KL\left(p_{\Theta(t_1)}\middle\|p_{\Theta(t_2)}\right)=\sum_{j=1}^{K}\pi_{j,t_1}\cdot\log\left(\frac{\pi_{j,t_1}}{\pi_{j,t_2}}\right)+\frac{1}{2}\times$$

$$\times\sum_{j}\left(tr\left(\Sigma_{j,t_2}^{-1}\cdot\Sigma_{j,t_1}\right)+\left(\mu_{j,t_2}-\mu_{j,t_1}\right)^{\top}\cdot\Sigma_{j,t_2}^{-1}\cdot\left(\mu_{j,t_2}-\mu_{j,t_1}\right)-d\right). \quad (13)$$

Degradation measurement is formalized through an expertly calibrated map of clusters and physical condition. This is accomplished by introducing a "degradation signature" vector ψ_j for the j-th cluster, defined by statistical features (e.g., high μ value, increased σ value, spectral energy shift to the high-frequency range), and an aggregated degradation assessment

$$G(t)=\sum_{j=1}^{K}\omega_j\cdot\Delta P_j(t)\cdot\langle\psi_j,1\rangle+\gamma\cdot\Delta\mu_{hot}(t), \quad (14)$$

where $\Delta P_j(t) = P_{j,t} - P_{j,t-\tau}$, ω_j are the weights determined by calibration (regression or Bayesian approximation) and $\Delta\mu_{hot}$ is the change in the mean in "hot" clusters. In the reference degradation labels presence, it is possible to estimate the regression model

$$s(t)\approx\beta^{\tau}\cdot\Phi(T),\quad \beta=arg\min_{\beta}\sum_{t}l\left(s(t),\beta^{\top}\cdot\Phi(t)\right)+\lambda\cdot\|\beta\|_2^2, \quad (15)$$

where $\Phi(t)$ is the aggregated cluster features set, and ℓ is the loss function (e.g., quadratic). It is noted that the method is robust to noise due to several design features:

1. Robust normalization and detrending eliminate low-frequency noise.
2. Including scaling coefficients and wavelet energies in the feature space facilitates the short-term spikes separation from background fluctuations.
3. Exponential forgetting λ allows the algorithm to adapt to long-term mode changes without retraining.
4. The procedures for creating or removing components provide mode "memory" and automatic adjustment of the clusters' number.

To detect sensor failures, smoothness and autocorrelation statistics are additionally calculated based on the condition that if ACF (S_n, 1) ≈ 1 and σ_n^2 is close to zero, the window is marked as suspicious and excluded from the contributions $P_{j,t}$ until the signal quality is confirmed.

The sensitivity and convergence analytical assessment is based on the fact that for a streaming gas temperature signal with a fine step η, the parameter estimates satisfy a stochastic approximation to the mixture maximum likelihood, assuming stationarity of the local interval. It is also noted that the adaptation rate is determined by λ and the effective samples' generalized size

$$N_{eff}=\frac{1}{1-\lambda}. \quad (16)$$

The computational complexity estimate per incoming milestone is based on computing the densities for all K components, which requires $O(K \cdot d^2)$ for storing and inverting covariances (or $O(K \cdot d)$ for diagonal approximation of Σ_j). Memory is then limited to $O(K \cdot d^2)$. Practical recommendations include choosing $d \ll m$ via feature selection or streaming PCA (online Oja [51]), where the principal component update is given by Oja's rule:

$$\omega_{t+1}=\omega_t+\eta_t\cdot\left(\phi_t-\omega_t\cdot\left(\omega_t^{\top}\cdot\phi_t\right)\right). \quad (17)$$

The developed methods' validation involves modeling the gas temperature values' degradation (with a linear or exponential shift of the mean and an increase in variance), injecting short-term anomalies, and validating on historical flight data with expert labeling. Evaluation metrics include

detection (average detection delay $\overline{\Delta}$), precision and recall, ROC-AUC for $A(\phi)$ rates, and the cluster structure (Silhouette, Adjusted Rand Index [52–54]) stability in the labeled intervals presence.

Thus, based on the above, Table 1 presents an algorithm for continuous clustering of short-term fluctuations in the helicopter TE gas temperature, including successive stages of streaming data reception, quality control and signal recovery, adaptive detrending and robust normalization, a window representation formation and a multifunctional feature extraction, online dimensionality reduction, incremental clustering with cluster life cycle management, the anomaly scoring calculation and the cluster structure evolution, as well as procedures for matching cluster signatures with physical signs of degradation and regulating alerts for assessing the turbine and compressor blades' condition.

Table 1
The training dataset fragment

Number	Step name	Short description (step function)	Output (note)
1	Input data and streaming reading	Continuous reception of scalar data and buffering for sliding windows.	Sliding window buffer, time metadata, provides a deterministic stream.
2	Signal quality control and restoration	Detection of gaps, artifacts, and measurement anomalies, imputation, or bad window marking.	Filtered or labeled signal, suspicious fragments marked.
3	Baseline extraction and detrending	Adaptive estimation of the mode's slow-time component and its removal to highlight short-term fluctuations.	Detrended time series, ready for local analysis.
4	Robust normalization	Local statistically robust normalization within a window to suppress outliers and account for regime transitions.	Normalized window fragments with reduced impact of outliers.
5	Window generation	Formation of fixed and/or multi-scale windows for subsequent feature extraction.	Windows ready sequence for feature generation.
6	Feature extraction	Feature set generation (statistics, instantaneous dynamics, spectral-wavelet characteristics, embedding dynamics, etc.).	Feature vectors for each window.
7	Stream dimensionality reduction	An online PCA or streaming feature selection use for dimensionality control and computational acceleration.	Compressed feature representation, reduced computational load.
8	Incremental clustering	A streaming clustering algorithm with exponential forgetting for updating cluster parameters in real time.	An up-to-date cluster model and assignments for incoming windows.

9	Cluster lifecycle management	Mechanisms for creating new clusters when new patterns appear and removing (aggregating) obsolete clusters.	Dynamically changing number of clusters, model drift-resistant.
10	Anomaly assessment and scoring	Calculation of anomaly rates based on cluster distance, density, and population frequency changes.	Anomaly rates for each window, input for alert rules.
11	Cluster evolution monitoring	Tracking assignment distributions, parameter drift, and stability metrics over time.	Time series of cluster shares and drift metrics.
12	Physical signature matching	alibration and maintenance of a “cluster-physical degradation signature” correspondence map for interpretation.	Correspondence map, interpretable degradation indicators.
13	Decision rules and alerts	Formalization of thresholds, aggregation rules, or learnable criteria for generating diagnostic alerts.	Diagnostic and predictive alerts, indicators for TR.
14	Fault tolerance and resource management	Sensor failure detection, computation redundancy, and load adaptation to onboard limitations.	Computational degradation modes, unreliable data flagging.
15	Adaptive calibration	Periodic or event-driven adjustments to map parameters and weights based on expert annotation.	Updated calibration parameters, false positives (false negatives) reduction.
16	Validation and reporting	Quality metrics collection (detection delay, precision, recall, cluster stability) and report generation for maintenance regulation.	Reports and metrics sets for performance evaluation and operational decision-making.

Thus, a streaming method for the short-term fluctuations’ continuous clustering in the helicopter TE gas temperature in front of the compressor turbines with a 0.5 Hz sampling frequency is proposed. This method includes robust preprocessing and detrending, multifunctional feature extraction, online dimensionality reduction, and incremental clustering with cluster lifecycle management for adaptation to operating mode transitions. The method provides a scalar anomaly estimate and an aggregated degradation metric, coupled with an expertly calibrated “cluster → physical signature” map, enabling early detection of turbine and compressor blade wear signs under limited onboard computing resources.

4. Case study and discussions

In this study, a numerical experiment was conducted using the developed method on the helicopter TE thermal dynamics under nominal conditions. The gas temperature in front of the compressor turbine $T_G(t)$, a real measurement series of the TV3-117 engine recorded by a standard onboard sensor on a production Mi-8MTV helicopter (Figure 1), was used. The sensor is a set of 14 dual chrome-alumel thermocouples of the T-102 type [55–57]. It is noted that the tests were carried out at the 2500-meter altitude under standard atmospheric conditions (air temperature ≈ 268 K, pressure ≈ 74 kPa). Signals were recorded at the Δt = 0.25 second interval (sampling frequency 4 Hz) for 320 seconds, which provided a 1280 readings sample.

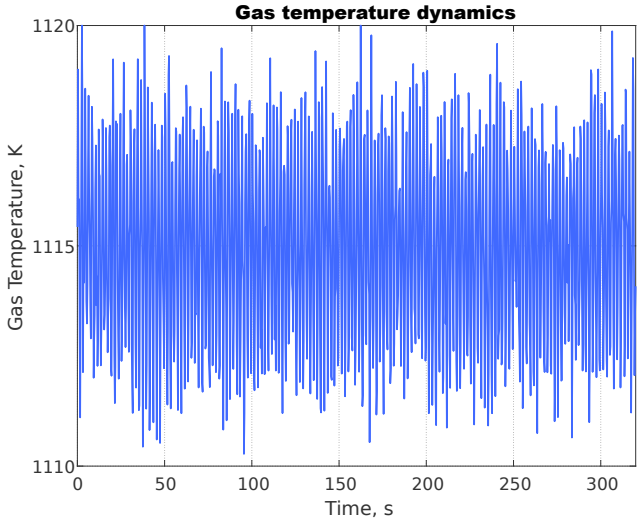

Figure 1: Diagram of the TV3-117 engines' gas temperature in front of the compressor turbine dynamics (initial diagram for forming the initial dataset). (author's development).

It is noted that Figure 1 shows a TV3-117 engine's gas temperatures in front of the compressor turbine time series with a 4 Hz sampling rate over a 0 to 320 seconds' range. The series' average temperature is approximately 1115 K, with measurements ranging from approximately 1090 to 1140 K. Against a weak low-frequency modulating trend background, a distinct high-frequency component is present, consisting of short-term oscillations with a typical amplitude of approximately 2 K and a characteristic period of approximately 5 seconds, manifested as regular "high-frequency" bursts.

A signal's pre-processing was performed by the onboard controller, and a two-stage filter was used to suppress interference. This filter included initial smoothing using the Savitzky-Golay method with an 11-sample window and a third-order polynomial. Outliers were then removed using a $\pm 3\sigma$ criterion, with gaps restored using linear interpolation. Systematic error correction took into account the thermocouples' calibration characteristics (with an error of no more than 1.5 K) and a correction for flow velocities up to 20 m/s. Gas temperature values were also normalized to a single scale using z-normalization:

$$z\left(T_G\right)_i = \frac{T_{G_{meas}}^{(i)} - \frac{1}{N}\cdot\sum_{i=1}^{N} T_{G_{meas}}^{(i)}}{\frac{1}{N}\cdot\sum_{i=1}^{N}\left(T_{G_{meas}}^{(i)} - \frac{1}{N}\cdot\sum_{i=1}^{N} T_{G_{meas}}^{(i)}\right)^2}, \tag{18}$$

where $T_{G_{meas}}^{(i)}$ is the i-th gas temperatures in front of the compressor turbine value recorded by the helicopter's standard sensor. Based on the above, normalized gas temperatures in front of the compressor turbine values hear were used to form the training dataset. This datasets' fragment is presented in Table 2.

Table 2
The training dataset fragment

Time, second	Gas temperature raw value, K	Gas temperature normalized value
0	1115,4	0,22527
...	...	...
40,031	1114,32	-0,44639
...	...	...
80,063	1115,25	0,13131
...	...	...
120,094	1115,12	0,05338
...	...	...
160,125	1115,03	-0,00612
...	...	...
199,906	1114,79	-0,15358
...	...	...
239,937	1115,22	0,11499
...	...	...
279,969	1115,77	0,45942
...	...	...
320	1114,74	-0,18315

To assess the training datasets' homogeneity, traditional metrics were used, including the number of observations, the mathematical expectation $\bar{x}$ and standard deviation σ, the skewness (SK) and kurtosis (KE) coefficients, the Shapiro-Wilk test (W and p-value) to check the distributions' normality, the Augmented Dickey-Fuller (Δy_t) and KPSS stationarity tests, the Ljung-Box $Q(h)$ test to identify autocorrelation, the Durbin-Watson (DW) statistic to assess the autocorrelation of residuals after detrending, the Levene test (W) to compare variances between segments, as well as segmental analysis of means and variances over equal sampling intervals [58–60]:

$$\bar{x}=\frac{1}{n}\cdot\sum_{i=1}^{n}x_i,\sigma=\sqrt{\frac{1}{n}\cdot\sum_{i=1}^{n}\left(x_i-\bar{x}\right)^2},SK=\frac{1}{n}\cdot\sum_{i=1}^{n}\left(\frac{x_i-\bar{x}}{\sigma}\right)^3,KE=\frac{1}{n}\cdot\sum_{i=1}^{n}\left(\frac{x_i-\bar{x}}{\sigma}\right)^4-3,$$

$$W=\frac{\left(\sum_{i=1}^{n}a_i\cdot x_{(i)}\right)^2}{\sum_{i=1}^{n}\left(x_i-\bar{x}\right)^2},\Delta y_t=\alpha+\beta\cdot t+\gamma\cdot y_{t-1}+\sum_{i=1}^{p}\delta_i\cdot\Delta y_{t-i}+\varepsilon_i, \quad (19)$$

$$KPSS=\frac{1}{n^2}\cdot\sum_{i=1}^{n}\frac{S_t^2}{\hat{\sigma}^2},S_t=\sum_{i=1}^{t}\hat{\varepsilon}_i,DW=\frac{\sum_{t=2}^{n}\left(e_t-e_{t-1}\right)^2}{\sum_{t=1}^{n}e_t^2},Q=n\cdot(n+2)\cdot\sum_{k=1}^{h}\frac{\hat{\rho}_k^2}{n-k},$$

$$W = \left(\frac{N-k}{k-1}\right) \cdot \frac{\sum_{j=1}^{k} n_j \cdot \left(\overline{Z}_{j\cdot} - \overline{Z}_{j\cdot\cdot}\right)^2}{\sum_{j=1}^{k} \sum_{i=1}^{n_j} \left(Z_{ij} - \overline{Z}_{j\cdot}\right)^2},$$

where $x(i)$ are ordered values, and the coefficients a_i depend on the expected values of the order statistics of the normal distribution, test hypothesis H_0: $\gamma = 0$ (a unit root presence); model $y_t = r_t + \varepsilon_t$, where r_t is a random walk, $\hat{\rho}_k$ is the estimated autocorrelation function, $Z_{ij} = \left|X_{ij} - \widetilde{X}_j\right|$; $\widetilde{X}_j$ i s the median of the j-th group.

Table 3 presents the training dataset's homogeneity evaluation numerical results, which include the sample size, the main moments of the distribution (mathematical expectation, standard deviation, skewness, and kurtosis coefficients), the statistical tests results for normality, stationarity, and autocorrelation (Shapiro–Wilk, ADF, KPSS, Ljung–Box, and Durbin–Watson), and the test for variances equality (Levene) with the corresponding statistics and p-values.

Table 3
The training dataset fragment

Metric	Value
Number of samples	1280
Mean, K	1115,4
Std (population), K	1,994
Skewness	-0,119
Excess kurtosis	0,285
Shapiro-Wilk (W)	0,994
Shapiro p-value	0,00001
ADF statistic	-6,080
ADF p-value	0
KPSS statistic	0,538
KPSS p-value	0,017
Ljung-Box Q(10)	110,558
Ljung-Box p-value	0
Durbin-Watson	0,320
Levene (W) (4 segments)	0,215
Levene p-value	0,837

According to Table 3, the training set is characterized by a mean of approximately 1115,43 Kelvin and a relatively small population variance ($\sigma \approx 1,99$ K). The skewness and kurtosis coefficients are close to zero, indicating that the distribution is close to normal. However, formal tests of normality yield conflicting results. The Shapiro-Wilk test rejects normality for the given sample (low p-value), while the distributions' moments are nearly symmetrical, which is a typical effect of large data datasets, in which small deviations from normality become statistically significant. Stationarity tests yield mixed results, according to which the ADF indicates a unit root (stationarity) absence, while the KPSS detects a possible deviation from stationarity, indicating the presence of a weak low-frequency trend or structural drift requiring detrending. The

Durbin-Watson statistic low value and the significant Ljung-Box test indicate a pronounced autocorrelation in the series. At the same time, the Levene test does not reveal statistically significant differences in variances between quartile segments, which confirms the relative homogeneity of the variance component over time.

In addition, Table 4 presents the dataset segmental analysis results across four equal intervals, namely, each segment's readings' initial and final indices, the average gas temperature level estimated values (Mean, K), and the corresponding variances (Var, K), which allow us to estimate the series' first and second moments' temporal homogeneity.

Table 4
The training dataset fragment

Segment	Start_idx	End_idx	Mean, K	Var, K
1	0	319	1115,5	1,702
2	320	639	1115,3	2,049
3	640	959	1115,4	2,084
4	960	1279	1115,3	1,799

Segment analysis (Table 4) shows that the estimated mean temperature levels in all four equal intervals are close to each other (the means spread does not exceed ≈ 0,26 K), indicating a stable baseline signal level and the absence of large-scale changes in operating modes in the observation interval under consideration. Segment variances are also within a narrow range (≈ 1,70…2,08 K2), while the observed minor increases in variability in the second and third segments indicate a local increase in short-term fluctuations rather than a systematic change in noise or a level shift. Taken together, these results confirm the time series' first and second moments' relative homogeneity, simultaneously emphasizing the need to apply locally adaptive normalization procedures and account for the variance of temporal variability when constructing stream clustering.

A study was conducted on continuous clustering of short-term fluctuations in exhaust gas temperature for a controlled scenarios set:

1. Nominal mode.
2. Increased noise level.
3. Slow average level drift.
4. Transient spikes.
5. Sensor "flatline" artifacts.
6. Regime change.

For each scenario, sliding window preprocessing, multifunctional feature extraction, streaming clustering, and cluster share evolution analysis were implemented to assess the method's sensitivity, robustness, and early detection of degradation indicators. The studies' results are shown in Figure 2.

The PCA projection shown in Figure 2a shows three relatively compact point clouds with partial overlap. One cluster is noted to occupy the central-lower region, while the other two are shifted to the left and upward along the PC axes. The resulting clustering structure indicates the presence of reproducible local patterns in the feature space under the nominal conditions. However, the projection shown in Figure 2b shows a noticeable expansion of the cluster clouds and an increase in overlapping zones, with one component acquiring a more extended distribution in the PC1 direction. The obtained clustering results indicate a decrease in cluster separability with increasing noise levels. The resulting clustering projection shown in Figure 2c demonstrates a

cluster's shift and partial separation along the PC axes. It is also noted that the clouds are partially located along the directional gradient of PC1, which is consistent with a slow trend presence in the features. The obtained results indicate that gradual changes in the mode manifest themselves as smooth motion in the feature space and can be detected by monitoring centroids or drift metrics. Figure 2d clearly shows individual outliers and distinct groups separated from the main body of observations. It is noted that these outliers form distinct clusters or tail branches in the projection. This behavior confirms the feature set's ability to identify short-term, high-amplitude events but also highlights the false-positive risk interpretations without additional aggregation logic based on duration and frequency of events. The PCA projection shown in Figure 2e contains a "compact dense cloud" corresponding to background variability and a separate compact cluster, which is a set of points separated in the feature space. The resulting cluster separation is consistent with the sensor's "sticking" period. It is noted that this distribution requires the diagnostic signal quality criteria to be used to distinguish true physical modes from measurement artifacts and to exclude artifactual clusters from the training set. The projection shown in Figure 2f reveals two adjacent but distinct regions, one of which contains dense clusters, while the other contains points shifted along PC1, which correlates with the modeled mean shift. The resulting cluster topology indicates the possibility of detecting mode changes based on distribution changes in the feature space and justifies the use of thresholds for changes in cluster proportions or centroid shift monitoring for rapid alerting.

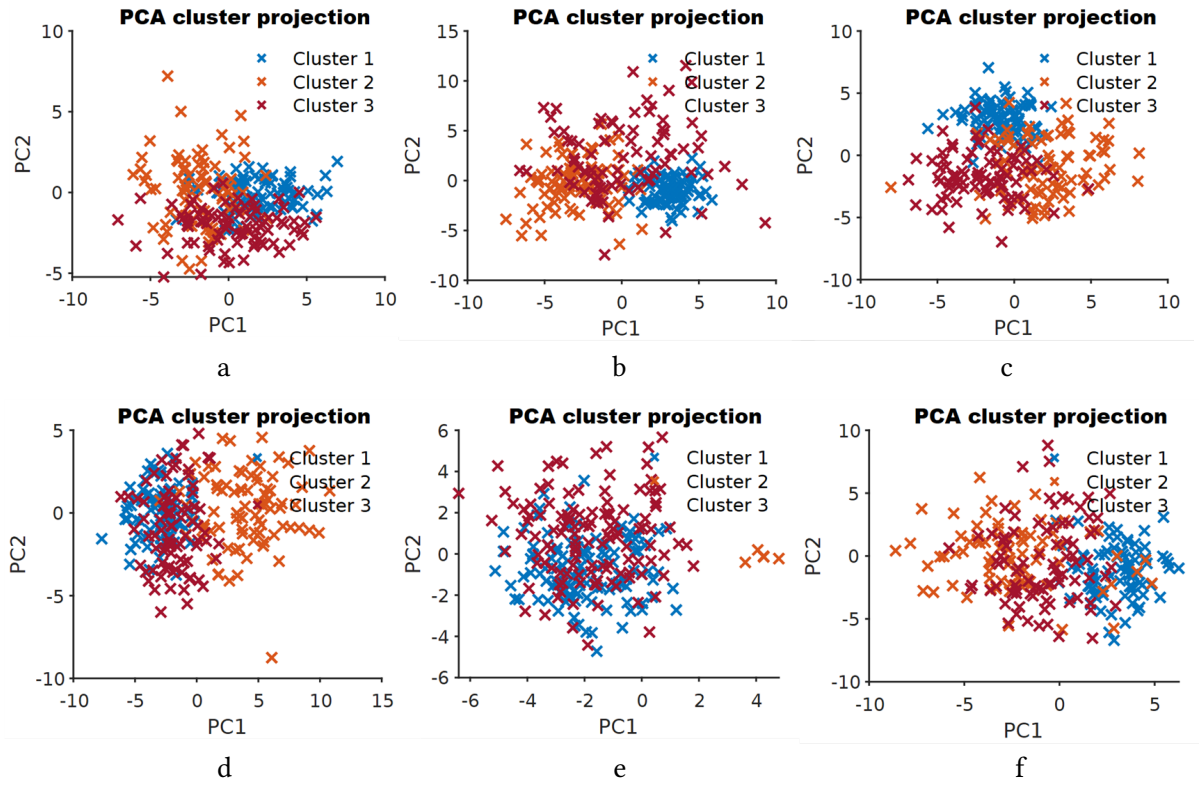

Figure 2: The gas temperature in front of the compressor turbine parameter values clustering results using the developed method: (a) Nominal mode; (b) Increased noise level; (c) Drift; (d) Transient spikes; (e) Flatline; (f) Regime change (author's development).

Based on the gas temperature in front of the compressor turbine parameter clustering, corresponding diagrams were obtained, which show characteristic patterns associated with a defect in the compressor turbine blades (Figure 3).

Thus, as a result of the developed continuous clustering method's experimental implementations, a defect detection in a first-stage turbine blade directly related to the compressor drive (the first turbine stage blade driving the compressor) is accomplished by identifying persistent or repeating assignments of sliding window feature vectors to a single cluster. This

“defective” cluster’s centroid is characterized by an elevated average window temperature and increased short-term variability, which corresponds to the physical mechanisms of localized overheating. In this context, the proposed defect types include fatigue or impact cracks in the leading edge and root joint, the working surfaces’ erosive abrasion, and the protective coatings’ localized loss (coating spallation), as well as an increase in the gap between the blade tip and the guide vanes due to wear. All of these defects lead to the heat transfers’ localized deterioration and the short-term “hot” events formation in the TG field. In feature space, this manifests as a separate, partially distant point cloud in the PCA projection, while in the time domain, it manifests as a short-term spike’s series and a subsequent increase in the assignments proportion to the “defective” cluster. For operational detection, a scalar indicator representing an assignment’s sliding proportion to the defective cluster was used, with a 0.20 empirical threshold. Exceeding this threshold over a certain number of sliding steps is considered a warning trigger. The proposed approach provides a balance between sensitivity and robustness to single outliers but requires explicitly adjusting the threshold based on historical degradation markers and accounting for the detection time delay due to the window length and aggregation step. It has been analytically shown that individual short-term spikes can generate false positives without additional logic for aggregation by frequency and duration of events, and a shift in the operating mode (drift or regime change) generates a centroids’ smooth movement in the feature space, which requires the detrending [61] or exponential “forgetting” [62] use during the cluster’s online updating.

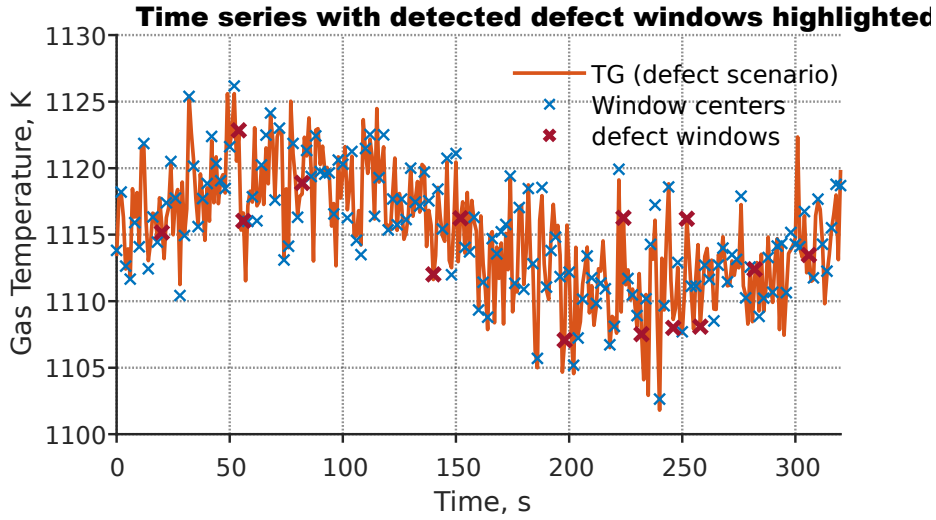

a

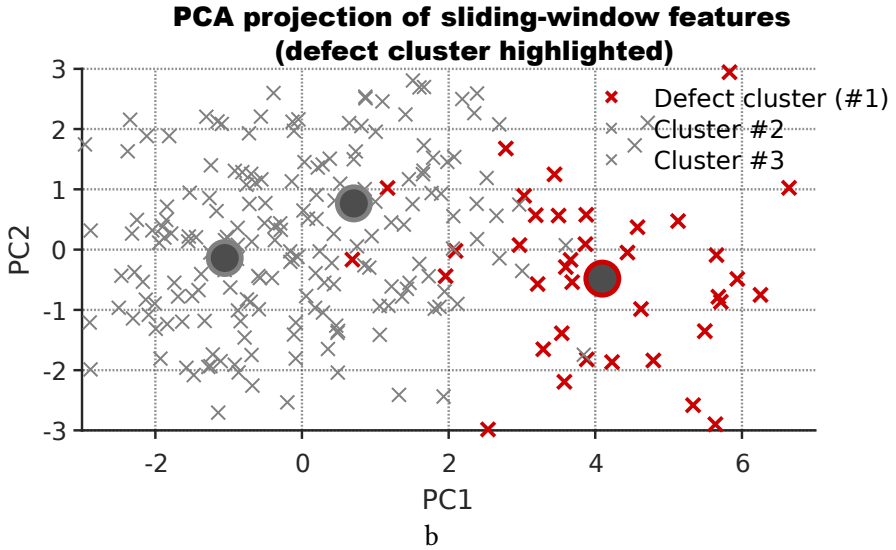

b

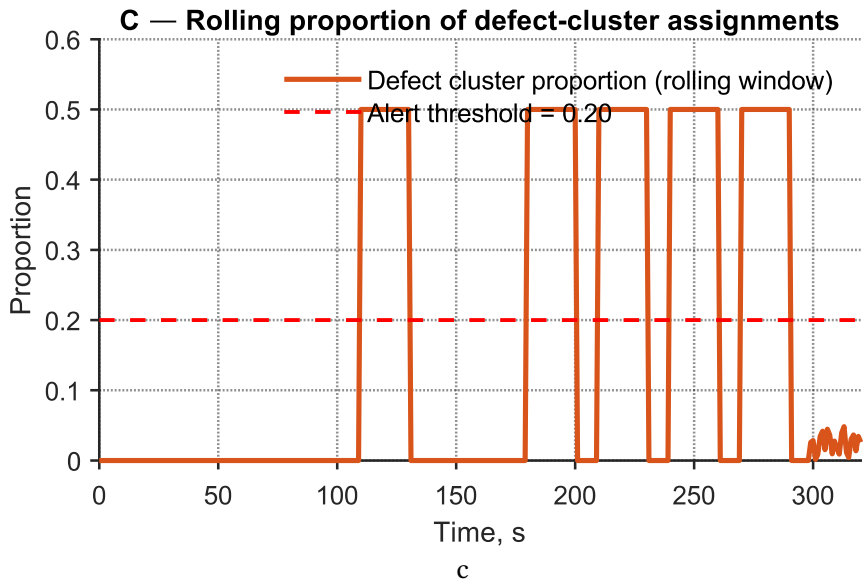

c

Figure 3: Results of compressor turbine defect detection based on the gas temperature in front of the compressor turbine parameters' values clustering: (a) Time series with highlighted windows assigned to the "defective" cluster; (b) The feature's PCA projection space with the highlighted defect cluster and the centroid's location; (c) The assignments proportion time series to the "defective" cluster with the alert threshold (author's development).

A comparative analysis (Table 5) shows that the developed streaming continuous clustering method occupies a practical niche between simple physical threshold approaches and resource-intensive deep learning models. The developed methods' application provides high potential for early detection of short-term patterns while being operationally compatible with online processing, while requiring minimal labeling and moderate computational costs.

Table 5
The comparative analysis results

Method	Online capability	Early detection	Marking required	Noise Resistance	Computational Cost
Developed streaming clustering method	High	High	Low (semi- or unsupervised)	Average	Medium
Physical threshold schemes	High	Low	No	Low	Low
Classical machine learning (regression, autoencoders, boosting)	Medium	Medium	Low-medium	Average	Medium
Deep networks (and digital twins)	Low (onboard)	High (during training)	High	Low-average	High
Matrix profile	Medium	High	Low	Average	Medium
Batch clustering (offline Kmeans, GMM)	Low	Low	Low	Low	Low

According to Table 5, the developed method's advantages over its closest analogues include adaptability to mode drift and interpretability through matching cluster signatures with physical degradation markers. These advantages are offset by moderate robustness to high noise levels and the need for signal quality control modules. It is noted that traditional threshold schemes are simple and interpretable but ineffective for short-term events. Deep models demonstrate high accuracy with large labeled datasets but are inapplicable to resource-constrained onboard electronics without significant optimization.

Based on the above, the practical recommendation is to use streaming clustering as an operational screening method, followed by verification through physical and statistical tests. In the labeled precedents' presence, it is necessary to use a retrospective confirmation model (DNN, digital twin [62–65]) to improve accuracy and reduce the false positive proportion.

It is also noted that the developed methods' practical limitations are related to the features and the clustering algorithm selected sets' sensitivity to the noise level and sensor artifacts (flatlines, sticking, etc.). Therefore, its implementation should include signal quality control procedures (dispersion and autocorrelation checks, flatline detection) and a cluster verification module using physically interpretable indicators (temperature markers, blade distribution, diagnostic measurements), as well as a calibration step on labeled degradation examples to evaluate ROC curves, select the optimal threshold, and determine the minimum warning stability time. Implementation into an onboard monitoring system requires preliminary sensitive parameter analysis (window length, step size, number of clusters, and fraction threshold), testing on synthetic defect injections, and adaptive recalibration procedure development for changing operating modes, taking into account computational limitations and latency requirements.

Thus, the streaming clustering with cluster lifecycle management and a physically based "cluster → defect" map combination is an important technical contribution, enabling early, robust, and interpretable detection of the helicopter TE compressor turbine blades degradations' initial stages within the onboard computing platforms' limitations.

5. Conclusions

A streaming method for continuous clustering of short-term gas temperature in front of the compressor turbine fluctuations of helicopter turboshaft engines has been developed, focused on streaming two-second measurements. The developed method consists of a processing pipeline. There are quality control and imputation, adaptive baseline detrending, robust local normalization, sliding window generation, multifunctional feature extraction (statistical moments, difference characteristics, short-term spectral-wavelet components), streaming dimensionality reduction, and incremental clustering with exponential "forgetting" and dynamic component lifecycle management. To translate statistical inferences into diagnostic solutions, an expert-calibrated "cluster ↔ physical degradation signature" map and an aggregated scalar degradation metric based on changes in the cluster assignments proportions are proposed. The developed method introduces several modification elements to ensure a balance between sensitivity to short-term patterns and robustness to single outliers:

1. A robust detrending and local MAD normalization integration for robustness to regime shifts.
2. A streaming clustering scheme with dynamic component creation or deletion mechanisms and exponential forgetting, ensuring adaptation to regime shift without batch retraining.
3. A combined anomaly score that takes into account the distance to the cluster centroid, cluster density, and cluster population rate variations.
4. Aggregation logic based on the assignment's sliding proportion to a defective cluster to reduce the number of false positives.

The developed method was validated using a real set of TV3-117 engine compressor turbine gas temperature measurements (Mi-8MTV flight recordings, 1280 samples at 4 Hz after preprocessing) and simulated scenarios, such as nominal mode, increased noise, slow drift, transient spikes, flatline artifacts, and mode transitions. The experiment revealed a reproducible "cluster" signature associated with the first-stage rotor blade degradations' initial stage. A defective cluster's centroid is characterized by an elevated average window temperature and increased short-term variability, forming a partially distant cloud in the PCA projection, while in the time domain, a short-term "hot" spike series and an increase in the assignments proportion are formed. The practical detection trigger is implemented as the defective assignments' sliding proportion excess above a 0.20 empirical threshold over a minimum number of windows. This criterion's introduction demonstrated the developed methods' ability to detect degradation departments earlier than traditional packet or threshold schemes, with acceptable resistance to single noise pulses.

Acknowledgements

The research was supported by the Ministry of Internal Affairs of Ukraine "Theoretical and applied aspects of the development of the aviation sphere" under Project No. 0123U104884.

Declaration on Generative AI

During this study preparation, the authors used ChatGPT-4.0, Gemini 2.5 flash, Grammarly to correct and improve the text quality, and also to eliminate grammatical errors. The authors have reviewed and edited the output and take full responsibility for this publications' content.

References

[1] W. Gao, M. Pan, W. Zhou, F. Lu, J.-Q. Huang, Aero-engine modeling and control method with model-based deep reinforcement learning, Aerospace 10 (3) (2023). doi:10.3390/aerospace10030209.

[2] T. Castiglione, D. Perrone, J. Song, L. Strafella, A. Ficarella, S. Bova, Linear model of a turboshaft aero-engine including components degradation for control-oriented applications, Energies 16 (6) (2023). doi:10.3390/en16062634.

[3] J. Song, Y. Wang, C. Ji, H. Zhang, Real-time optimization control of variable rotor speed based on Helicopter/ turboshaft engine on-board composite system, Energy 301 (2024). doi:10.1016/j.energy.2024.131701.

[4] S. Vladov, Y. Shmelov, R. Yakovliev, M. Petchenko, S. Drozdova, Neural network method for helicopters turboshaft engines working process parameters identification at flight modes, in: Proceedings of the 2022 IEEE 4th International Conference on Modern Electrical and Energy System, MEES '2022, IEEE, New York, NY, 2022, pp. 604–609. doi:10.1109/MEES58014.2022.10005670.

[5] M. Chen, K. Zhang, H.-L. Tang, A probabilistic design methodology for a turboshaft engine overall performance analysis, Adv. Mech. Eng. 6 (2014). doi:10.1155/2014/976853.

[6] Z. Gu, Q. Li, S. Pang, W. Zhou, J. Wu, C. Zhang, Turbo-shaft engine adaptive neural network control based on nonlinear state space equation, Chinese Journal of Aeronautics 37 (4) (2024) 493–507. doi:10.1016/j.cja.2023.08.012.

[7] G. Li, L. Zhang, G. Xia, S. Li, Structural reliability analysis of aero-engine turbine components based on particle swarm optimization back propagation neural network, Appl. Sci. 15 (6) (2025). doi:10.3390/app15063160.

[8] F. Liu, J. Yang, Q. Wang, Y. Liu, H. Wang, In-situ noncontact measurement system for nozzle throat deformation in high-temperature gas heating via laser speckle digital image correlation with wavelet smoothing of displacement field, Measurement 201 (2022). doi:10.1016/j.measurement.2022.111696.

[9] Q. Kang, H. Ji, Y. Yuan, Y. Ye, Autonomous helicopter shipboard recovery flight control design based on tau theory, Aerosp. Sci. Technol. 159 (2025). doi:10.1016/j.ast.2025.109956.
[10] S. Yepifanov, O. Bondarenko, Development of turboshaft engine adaptive dynamic model: Analysis of estimation errors, Trans. Aerosp. Res. 2022 (4) (2022) 59–71. doi:10.2478/tar-2022-0024.
[11] J. Hu, Y. Yang, N. Hu, X. Lin, Dynamic modeling and characteristic analysis of a helicopter main reducer for tooth crack diagnosis, Measurement 247 (2025). doi:10.1016/j.measurement.2025.116823.
[12] S. Vladov, Y. Shmelov, R. Yakovliev, M. Petchenko, Helicopters turboshaft engines parameters identification using neural network technologies based on the Kalman filter, in: Proceedings of the 18th International Conference of Information and Communication Technologies in Education, Research, and Industrial Applications, ICTERI ’2023, Springer, Cham, Switzerland 2023, pp. 82–97. doi:10.1007/978-3-031-48325-7_7.
[13] Y. Tan, Y. Chen, Y. Zhao, M. Liu, Z. Wang, L. Du, C. Wu, X. Xu, Recent advances in signal processing algorithms for electronic noses, Talanta 283 (2025). doi:10.1016/j.talanta.2024.127140.
[14] K. V. Santhosh, B. K. Roy, An intelligent temperature measurement technique using J type thermocouple with an optimal neural network, Sensors and Transducers, 147 (12) (2012), 6–14.
[15] F. Liu, J. Yang, Q. Wang, Y. Liu, H. Wang, In-situ noncontact measurement system for nozzle throat deformation in high-temperature gas heating via laser speckle digital image correlation with wavelet smoothing of displacement field, Measurement 201 (2022). doi:10.1016/j.measurement.2022.111696.
[16] C. Hu, K. Miao, M. Zhou, Y. Shen, J. Sun, Intelligent performance degradation prediction of light-duty gas turbine engine based on limited data, Symmetry 17 (2) (2025). doi:10.3390/sym17020277.
[17] M. Pasieka, N. Grzesik, K. Kuźma, Simulation modeling of fuzzy logic controller for aircraft engines, Int. J. Comput. 16:1 (2017) 27–33. doi:10.47839/ijc.16.1.868.
[18] S. J. Mohammadi, S. A. M. Fashandi, S. Jafari, T. Nikolaidis, A scientometric analysis and critical review of gas turbine aero-engines control: From Whittle engine to more-electric propulsion, Measurement and Control 54 (5–6) (2021) 935–966. doi:10.1177/0020294020956675.
[19] Z. Zhao, Y. Sun, J. Zhang, Fault detection and diagnosis for sensor in an aero-engine system, in: Proceedings of the 2016 Chinese Control and Decision Conference, CCDC ’2016, IEEE, New York, NY, 2014, pp. 2977–2982. doi:10.1109/ccdc.2016.7531492.
[20] Y. Yin, X. Heng, H. Zhang, A. Wang, Modeling method and dynamic analysis of turboshaft engine combustor rotor with curvic couplings considering thermal contact resistance under temperature field influence, Results in Engineering 25 (2025). doi:10.1016/j.rineng.2024.103853.
[21] S. Yepifanov, Aircraft turbine engine automatic control based on adaptive dynamic models, Trans. Aerosp. Res. 2020 (4) (2020) 61–70. doi:10.2478/tar-2020-0021.
[22] H. Aygun, Thermodynamic, environmental and sustainability calculations of a conceptual turboshaft engine under several power settings, Energy 245 (2022). doi:10.1016/j.energy.2022.123251.
[23] P. C. Lallana, G. Aldabaldetreku, A. López, D. S. Montero, G. Durana, J. Mateo, M. Á. Losada, J. Zubia, C. Vázquez, Sensing applications in aircrafts using polymer optical fibres, Sensors 21 (11) (2021). doi:10.3390/s21113605.
[24] T. Liu, L. Gao, R. Li, Experimental data-driven flow field prediction for compressor cascade based on deep learning and ℓ1 regularization, J. Therm. Sci. 33 (2024) 1867–1882. doi:10.1007/s11630-024-2035-8.
[25] K. Wang, A. He, J. Liu, Q. Zhou, Z. Hu, An online learning framework for aero-engine sensor fault detection isolation and recovery, Aerosp. Sci. Technol. 162 (2025). doi:10.1016/j.ast.2025.110241.

[26] S. Cao, H. Zuo, X. Zhao, C. Xia, Real-time gas path fault diagnosis for aeroengines based on enhanced state-space modeling and state tracking, Aerospace 12 (7) (2025). doi:10.3390/aerospace12070588.
[27] W. Gao, M. Pan, W. Zhou, F. Lu, J.-Q. Huang, Aero-engine modeling and control method with model-based deep reinforcement learning, Aerospace 10 (3) (2023). doi:10.3390/aerospace10030209.
[28] Z. Wei, S. Zhang, S. Jafari, T. Nikolaidis, Gas turbine aero-engines real time on-board modelling: A review, research challenges, and exploring the future, Prog. Aerosp. Sci. 121 (2020). doi:10.1016/j.paerosci.2020.100693.b
[29] M. de Castro-Cros, M. Velasco, C. Angulo, Machine-learning-based condition assessment of gas turbines — A review, Energies 14 (24) (2021). doi:10.3390/en14248468.
[30] H. Chen, Q. Li, Z. Ye, S. Pang, Neural network-based parameter estimation and compensation control for time-delay servo system of aeroengine, Aerospace 12 (1) (2025). doi:10.3390/aerospace12010064.
[31] X. Chang, J. Huang, F. Lu, Sensor fault tolerant control for aircraft engines using sliding mode observer, Energies 12 (21) (2019). doi:10.3390/en12214109.
[32] W. Cui, R. Wang, T. Sun, Z. Liu, Managing remaining useful life of cyber-aeroengine systems using a graph spatio-temporal attention recurrent network with phase-lag index, Energy 308 (2024). doi:10.1016/j.energy.2024.132924.
[33] H. Zhao, X. Lin, Z. Liao, M. Xu, Y. Yao, B. Duan, Z. Song, Highly fault-tolerant thrust estimation for gas turbine engines via feature-level dissimilarity design, Measurement 244 (2025). doi:10.1016/j.measurement.2024.116350.
[34] S. Vladov, A. Banasik, A. Sachenko, W. M. Kempa, V. Sokurenko, O. Muzychuk, P. Pikiewicz, A. Molga, V. Vysotska, Intelligent method of identifying the nonlinear dynamic model for helicopter turboshaft engines, Sensors 24 (19) (2024). doi:10.3390/s24196488.
[35] S. Du, W. Han, Z. Kang, F. Luo, Y. Liao, and Z. Li, A peak-finding siamese convolutional neural network (PF-SCNN) for aero-engine hot jet FT-IR spectrum classification, Aerospace 11 (9) (2024). doi:10.3390/aerospace11090703.
[36] J. Zou, P. Lin, Multichannel attention-based TCN-GRU network for remaining useful life prediction of aero-engines, Energies 18 (8) (2025). doi:10.3390/en18081899.
[37] S. Vladov, V. Vysotska, V. Sokurenko, O. Muzychuk, M. Nazarkevych, V. Lytvyn, Neural network system for predicting anomalous data in applied sensor systems, Appl. Syst. Innov. 7 (5) (2024). doi:10.3390/asi7050088.
[38] D. Chumachenko, O. Sokolov, S. Yakovlev, Fuzzy recurrent mappings in multiagent simulation of population dynamics systems, Int. J. Comput. 19 (2) (2020) 290–297. doi:10.47839/ijc.19.2.1773.
[39] J. Rabcan, V. Levashenko, E. Zaitseva, M. Kvassay, S. Subbotin, Non-destructive diagnostic of aircraft engine blades by Fuzzy Decision Tree, Engineering Structures 197 (2019). doi:10.1016/j.engstruct.2019.109396.
[40] X. Han, J. Huang, X. Zhou, Z. Zou, F. Lu, W. Zhou, A novel, reduced-order optimization method for nonlinear model correction of turboshaft engines, J. Mech. Sci. Technol. 38 (4) (2024) 2103–2122. doi:10.1007/s12206-024-0340-5.
[41] S. Shivansh, P. Akash Kumar, S. Sharanya, Predicting aircraft turbofan engine degradation with recurrent neural networks, in: Proceedings of the 2024 IEEE International Conference on Information Technology, Electronics and Intelligent Communication Systems, ICITEICS '2024, IEEE, New York, NY, 2024, pp. 304–309. doi:10.1109/ICITEICS61368.2024.10625502.
[42] H.-J. Jin, Y.-P. Zhao, M.-N. Pan, A novel method for aero-engine time-series forecasting based on multi-resolution transformer, Expert Syst. Appl. 255 (2024). doi:10.1016/j.eswa.2024.124597.
[43] S. Tovkach, Wireless-based information model of the common operation of the elements of the aviation gas turbine engine, Aviation 28 (3) (2024) 141–147. doi:10.3846/aviation.2024.22143.

[44] W. Liu, G. Xu, X. Gu, J. Yao, M. Li, M. Lei, Q. Chen, Y. Fu, Experimental analysis and thermodynamic modeling for multilevel heat exchange system with multifluid in aero engines. Energy 315 (2025). doi:10.1016/j.energy.2025.134373.

[45] A. R. Marakhimov, K. K. Khudaybergenov, Approach to the synthesis of neural network structure during classification, Int. J. Comput. 19 (1) (2020) 20–26. doi:10.47839/ijc.19.1.1689.

[46] V. Hamolia, V. Melnyk, P. Zhezhnych, A. Shilinh, Intrusion detection in computer networks using latent space representation and machine learning. Int. J. Comput. 19 (3) (2020) 442–448. doi:10.47839/ijc.19.3.1893.

[47] I. Perova, Y. Bodyanskiy, Fast medical diagnostics using autoassociative neuro-fuzzy memory, International Journal of Computing 16 (1) (2017) 34–40. doi:10.47839/ijc.16.1.869.

[48] I. Perova, Y. Bodyanskiy, Adaptive human machine interaction approach for feature selection-extraction task in medical data mining, Int. J. Comput. 17 (2) (2018) 113–119. doi:10.47839/ijc.17.2.997.

[49] S. Vladov, Y. Shmelov, R. Yakovliev, Optimization of helicopters aircraft engine working process using neural networks technologies, in: Proceedings of the 6th International Conference on Computational Linguistics and Intelligent Systems (COLINS 2022). Volume I: Main Conference, COLINS '2022, CEUR Workshop Proceedings, Aachen, Germany, 2022, pp. 1639–1656.

[50] G. E. Ceballos Benavides, M. A. Duarte-Mermoud, L. B. Martell, Control error convergence using Lyapunov direct method approach for mixed fractional order model reference adaptive control, Fractal Fract. 9 (2) (2025). doi:10.3390/fractalfract9020098.

[51] Z. Hu, E. Kashyap, O. K. Tyshchenko, GEOCLUS: A fuzzy-based learning algorithm for clustering expression datasets, in: Proceedings of the Fifth International Conference on Computer Science, Engineering, and Education Applications, ICCSEEA '2022, Springer, Cham, Switzerland, 2022, pp. 337–349. doi:10.1007/978-3-031-04812-8_29.

[52] N. Shakhovska, V. Yakovyna, N. Kryvinska, An improved software defect prediction algorithm using self-organizing maps combined with hierarchical clustering and data preprocessing, in: Proceedings if the of the 31st International Conference on Database and Expert Systems Applications, DEXA '2020, Springer, Cham, Switzerland, 2020, pp. 414–424. doi:10.1007/978-3-030-59003-1_27.

[53] P. Cosenza, A.-L. Fauchille, D. Prêt, S. Hedan, A. Giraud, Statistical representative elementary area of shale inferred by micromechanics, Int. J. Eng. Sci. 142 (2019) 53–73. doi:10.1016/j.ijengsci.2019.05.012.

[54] C. M. Stefanovic, A. G. Armada, X. Costa-Perez, Second order statistics of Fisher-Snedecor distribution and their application to burst error rate analysis of multi-hop communications, IEEE Open J. Commun. Soc. 3 (2022) 2407–2424. doi:10.1109/ojcoms.2022.3224835.

[55] S. Vladov, R. Yakovliev, O. Hubachov, J. Rud, Neuro-fuzzy system for detection fuel consumption of helicopters turboshaft engines, in: Proceedings of the 3rd International Workshop on Information Technologies: Theoretical and Applied Problems 2023, ITTAP '2023, CEUR Workshop Proceedings, Aachen, Germany, 2024, pp. 55–72.

[56] S. Vladov, R. Yakovliev, O. Hubachov, J. Rud, S. Drodova, A. Perekrest, Modified discrete neural network PID controller for controlling the helicopters turboshaft engines free turbine speed, in: Proceedings of the 2023 IEEE 5th International Conference on Modern Electrical and Energy System, MEES '2023, IEEE, New York, NY, 2023. pp. 797–802. doi:10.1109/MEES61502.2023.10402433.

[57] S. Vladov, Y. Shmelov, R. Yakovliev, M. Petchenko, Modified neural network fault-tolerant closed onboard helicopters turboshaft engines automatic control system, in: Proceedings of the 7th International Conference on Computational Linguistics and Intelligent Systems. Volume I: Machine Learning Workshop, CoLInS '2023, CEUR Workshop Proceedings, Aachen, Germany, 2023, pp. 160–179.

[58] B. Rusyn, R. Kosarevych, O. Lutsyk, V. Korniy, Segmentation of atmospheric clouds images obtained by remote sensing, in: Processing of the 2018 14th International Conference on

Advanced Trends in Radioelecrtronics, Telecommunications and Computer Engineering, TCSET ’2018, IEEE, New York, NY, 2018, pp. 213–216. doi:10.1109/tcset.2018.8336189.

[59] R. Donida Labati, A. Genovese, E. Muñoz, V. Piuri, F. Scotti, G. Sforza, Computational intelligence for biometric applications: A survey, Int. J. Comput. 15 (1) (2016) 40–49. doi:10.47839/ijc.15.1.829.

[60] B. Rusyn, I. Prudyus, V. Ostap, Fingerprint image enhancement algorithm, in: Processing of the 6th International Conference of the Experience of Designing and Application of CAD Systems in Microelectronics, CADSM ’2001, IEEE, New York, NY, 2001, pp. 193–194. doi:10.1109/CADSM.2001.975804.

[61] Y. Varetskyy, B. Rusyn, A. Molga, A. Ignatovych, A new method of fingerprint key protection of grid credential, Advances in Intelligent and Soft Computing 84 (2010) 99–103. doi:10.1007/978-3-642-16295-4_11.

[62] F. Geche, A. Batyuk, O. Mulesa, V. Voloshchuk, The combined time series forecasting model, in: Proceedings of the 2020 IEEE Third International Conference on Data Stream Mining & Processing, DSMP ’2020, IEEE, New York, NY, 2020, pp. 272–275. doi:10.1109/dsmp47368.2020.9204311.

[63] V. Kovtun, I. Izonin, M. Gregus, Model of functioning of the centralized wireless information ecosystem focused on multimedia streaming, Egypt. Inform. J. 23 (4) (2022) 89–96. doi:10.1016/j.eij.2022.06.009.

[64] B. Tarle, M. Akkalaksmi, Improving classification performance of neuro-fuzzy classifier by imputing missing data, Int. J. Comput. 18 (4) (2019) 495–501. doi:10.47839/ijc.18.4.1619.

[65] O. Bisikalo, O. Danylchuk, V. Kovtun, O. Kovtun, O. Nikitenko, V. Vysotska, Modeling of operation of information system for critical use in the conditions of influence of a complex certain negative factor, Int. J. Control Autom. Syst. 20 (6) (2022) 1904–1913. doi:10.1007/s12555-021-0368-6.